Optical Emission and Absorption Studies of Silver Atoms in Rare Gas Matrices at 12 K; Silver Atom Cryophotoaggregation

S. A. Mitchell, J. Farrell, G. A. Kenney-Wallace,* and G. A. Ozin*

Contribution from the Department of Chemistry, University of Toronto, Toronto, Ontario, Canada M5S 1A1. *Received January 18, 1980*

Abstract: The fluorescence spectra of silver atoms isolated in Ar, Kr, and Xe matrices at 12 K, excited at the $^2P \leftarrow {}^2S$ resonance absorption frequencies, show a number of intense bands with spectral shifts in the range 6–16 $cm^{-1} \times 10^3$, depending on the matrix support. A comprehensive study of the effects of the matrix conditions on the emission spectra is reported. The spectra are in all cases very sensitive to the density of silver atoms, matrix temperature, exposure to UV radiation, and thermal annealing. The preliminary results of a time-resolved study of the Ag/Xe emission bands are also described. Prolonged UV photolysis at the absorption frequencies promotes diffusion and aggregation of the silver atoms. The relationship between the optical and photolytic properties is discussed, and an interpretation is given in terms of a vibronic coupling model involving the Jahn–Teller effect.

Introduction

There is now a significant body of spectroscopic evidence to indicate that there are strong guest–host interactions when certain metal atoms are embedded in rare gas matrices at low temperature.[1-5] For silver atoms entrapped in Ar, Kr, and Xe matrices at 12 K, it has been demonstrated that continuous broad-band UV excitation of the $5p^1\ ^2P \leftarrow 5s^1\ ^2S$ atomic absorption lines produces intense luminescence bands exhibiting large spectral red shifts[2] and promotes diffusion and aggregation of the silver atoms.[6,7] These photoinduced clustering processes have been observed for several other metal atomic species in rare gas matrices, including Cu,[8] Cr,[9] Mo,[9] Ni,[10] Rh,[11a] and Na.[11b] It is therefore of interest to investigate the details of the operative guest–host interactions, as a function of both the metal atom and the matrix, in order to develop a general model which can account for both the energetics and dynamics of these optically excited systems. We report here an extensive study of the absorption, fluorescence, and excitation spectra of silver atoms at various densities in rare gas matrices at 12 K, together with fluorescence depolarization measurements and the preliminary data from the first, time-resolved study of the emission lifetimes of silver atoms excited in a Xe matrix.

Whereas the $5p^1\ ^2P \leftarrow 5s^1\ ^2S$ optical transition of free silver atoms appears as a spin–orbit doublet ($^2P_{1/2,3/2}$),[12] the corresponding transition of silver atoms isolated in well-annealed rare gas matrices shows a threefold splitting of the absorption band.[13] The additional splitting in the matrix spectra has been rationalized by Forstmann et al.[13] in terms of a static crystal field interaction. Although the crystal field analysis provides a satisfactory explanation for the structure of the absorption spectra, it would appear that additional concepts are required to account for the luminescent and photolytic properties. We outline in this paper a vibronic coupling model, which is based on the Jahn–Teller effect and which encompasses both the absorption and emission properties of the silver system. Although this effect is frequently invoked to explain splittings in the absorption spectra of matrix-isolated metal atoms,[14,20] it is nevertheless difficult to directly prove. However, recent optical absorption and magnetic circular dichroism studies,[14a] together with earlier ESR evidence,[5] present convincing evidence for the importance of the Jahn–Teller effect in matrix-isolated excited-state Mg and ground-state Al and Ga atoms, respectively.

Luminescence spectra have previously been reported for a limited number of matrix-isolated metal atomic species, including Li,[14b] Na,[3a] K,[3b] Rb,[15] Ca,[4] Ti,[16] Nb,[17] Au,[2b] and Ag.[2] The spectra obtained for the alkali-like metal atoms exhibit large red shifts in all cases. Only in the case of Li atoms in rare gas matrices has the Jahn–Teller effect been suggested[14b] to account for the observed luminescent properties. It is probable that the analysis reported herein for silver atoms can be extended to include some of the other alkali-like systems, since generally similar optical absorption and emission properties have been observed within this group.

Experimental Section

Monatomic silver vapor was generated by directly heating a tantalum filament around the center of which was wound 0.010-in. diameter silver wire (99.999%, supplied by Imperial Smelting Co., Toronto). Research grade argon, krypton, and xenon gases were supplied by Matheson of Canada. The rate of Ag atom deposition was continuously monitored by using a quartz crystal microbalance built into the furnace–cryostat assembly.[18] Matrices were deposited onto a NaCl optical window cooled to 12 K by means of an Air Products Displex closed-cycle helium refrigerator. UV–visible spectra were recorded on a Unicam SP 8000 spectrophotometer in the range 200–700 nm.

Emission spectra were recorded on a Perkin-Elmer MPF 44 fluorescence spectrometer, selecting both the excitation wavelength (λ_{ex}) and emission wavelength (λ_f) with scanning monochromators. The excitation beam was defocused (to avoid excessive photobleaching) by removing the lens in the sample compartment. Scattered light was minimized by the

* Address correspondence to the authors at Lash Miller Chemical Laboratories.

(1) Gruen, D. M. In "Cryochemistry"; Moskovits, M., Ozin, G. A., Eds.; Wiley: New York, 1976; Chapter 10.
(2) (a) Kolb, D. M.; Leutloff, D. *Chem. Phys. Lett.* **1978**, *55*, 264. (b) Leutloff, D.; Kolb, D. M. *Ber. Bunsenges. Phys. Chem.* **1979**, *83*, 666.
(3) (a) Balling, L. C.; Havey, M. D.; Dawson, J. F. *J. Chem. Phys.* **1978**, *69*, 1670. (b) Balling, L. C.; Havey, M. D.; Wright, J. J. *Ibid.* **1979**, *70*, 2404.
(4) Bondybey, V. E. *J. Chem. Phys.* **1978**, *68*, 1308.
(5) Ammeter, J. H.; Schlosnagle, D. C. *J. Chem. Phys.* **1973**, *59*, 4784.
(6) Ozin, G. A.; Huber, H. *Inorg. Chem.* **1978**, *17*, 155.
(7) Mitchell, S. A.; Ozin, G. A. *J. Am. Chem. Soc.* **1978**, *100*, 6776.
(8) Ozin, G. A.; Huber, H.; McIntosh, D.; Mitchell, S. A.; Norman, J. G., Jr.; Noodleman, L. *J. Am. Chem. Soc.* **1979**, *101*, 3504.
(9) (a) Ozin, G. A.; Klötzbucher, W. *J. Mol. Catal.* **1977**, *3*, 195. (b) Ozin, G. A.; Klötzbucher, W. *J. Am. Chem. Soc.* **1978**, *100*, 2262; *Inorg. Chem.* **1979**, *18*, 2101.
(10) Ozin, G. A. *Catal. Rev. Sci. Eng.* **1977**, *16*, 191.
(11) (a) Ozin, G. A.; Hanlan, A. J. Lee, *Inorg. Chem.* **1979**, *18*, 1781. (b) Ozin, G. A.; Huber, H. *Inorg. Chem.* **1979**, *18*, 1402.
(12) Moore, C. E. *Natl. Bur. Stand. (U.S.), Circ.* **1958**, *No. 467* (Vol. II, III).
(13) Forstmann, F.; Kolb, D. M.; Leutloff, D.; Schülze, W. *J. Chem. Phys.* **1977**, *66*, 2806.
(14) (a) Mowery, R. L.; Miller, J. C.; Krausz, E. R.; Schatz, P. N.; Jacobs, S. M.; Andrews, L. *J. Chem. Phys.* **1979**, *70*, 3920. (b) Belyaeva, A. A.; Predtechenskii, Y. B.; Shcherba, L. D. *Opt. Spectrosc. (Engl. Transl.)* **1973**, *34*, 21. (c) McCarty, M., Jr.; Robinson, G. W. *Mol. Phys.* **1959**, *2*, 415.
(15) Micklitz, H.; Luchner, K. *Z. Phys.* **1974**, *270*, 79.
(16) Gruen, D. M.; Carstens, D. J. W. *J. Chem. Phys.* **1971**, *54*, 5206.
(17) Green, D. W.; Gruen, D. M. *J. Chem. Phys.* **1972**, *57*, 4462.
(18) Moskovits, M.; Ozin, G. A. *Appl. Spectrosc.* **1972**, *26*, 487.

0002-7863/80/1502-7702$01.00/0

Table I. Absorption Spectra of Silver Atoms in Rare Gas Matrices at 12 K

matrix	abs max, nm
Ar	299, 304, 315
Kr	309, 313, 322
Xe	322, 326, 327, 335
gas phase[a]	3?8, 338

[a] Reference 12.

Table II. Major Emission Bands of Ag Atoms in Ar, Kr, and Xe Matrices

emission max, nm	bandwidth (fwhm), $cm^{-1} \times 10^3$	energy shift,[a] $cm^{-1} \times 10^3$
	Ar	
326	0.35	2.77
367	1.60	6.20
423	-	9.80
457	-	11.56
478	~0.9	12.52
	Kr	
328	~0.4	1.87
415	1.53	8.27
495	~1.3	12.16
525	-	13.31
	Xe	
480[b]	~1.3	10.22
550	1.79	12.87
680	1.56	16.35

[a] The difference in energy between the highest energy excitation (299 nm/Ar, 309 nm/Kr, 322 nm/Xe) and the corresponding emission maxima. [b] Appears only under high concentration conditions.

use of isolating filters, and control spectra were taken of rare gas matrices in the *absence* of Ag atoms, in order to monitor background scatter from the cell itself or impurity emission. These effects proved to be small and comprised <1% of the observed emission signal. Excitation spectra were obtained by observing the emission intensity at a given λ_f and scanning the excitation wavelength, λ_{ex}. The excitation and emission spectra were corrected for the frequency dependence of the excitation intensity; however, the emission spectra were not corrected for the characteristics of the analyzing monochromator and photomultiplier. Polarization studies were made in situ in the fluorescence spectrometer by using thin-film polarizers to select out the desired polarization components of the exciting and fluorescence wavelengths.

The time-resolved, lifetime measurements were carried out in the Ag/Xe matrix by exciting the Ag atoms with a nanosecond, UV laser pulse. The 8 ns (fwhm) laser pulse at 337.1 nm from a 5 Hz, MWatt Blumlein nitrogen laser was directed onto the sample in the cryogenic cell through a series of narrow band-pass filters and beam attenuators (to avoid scattered light and photobleaching). The sample fluorescence was collected with a lens and focused onto the slits of a monochromator and 1P28 photomultiplier, coupled through 50 Ω to a Tektronix 475 oscilloscope. The resulting emission signals were recorded on ASA 410 Polaroid film. The response of the detection system was ~3 ns. Full details of the laser system will appear elsewhere.[19]

Results

1. Absorption and Emission Spectra. The absorption spectra for Ag atoms isolated in freshly deposited Ar, Kr, and Xe matrices are shown as inserts in Figure 1, and the wavelengths of the absorption maxima are listed in Table I. Note the threefold splitting of the $^2P \leftarrow {}^2S$ resonance line[13] and the presence of weak side bands at lower energy in all cases. Under higher resolution a fourth major absorption band appears in Ag/Xe near 326 nm; no corresponding band appears in Ar or Kr matrices.[21]

Representative emission spectra for Ag atoms trapped in Ar, Kr, and Xe matrices, excited at λ_{ex} corresponding to the major absorption maxima, are displayed in Figure 1, and the properties

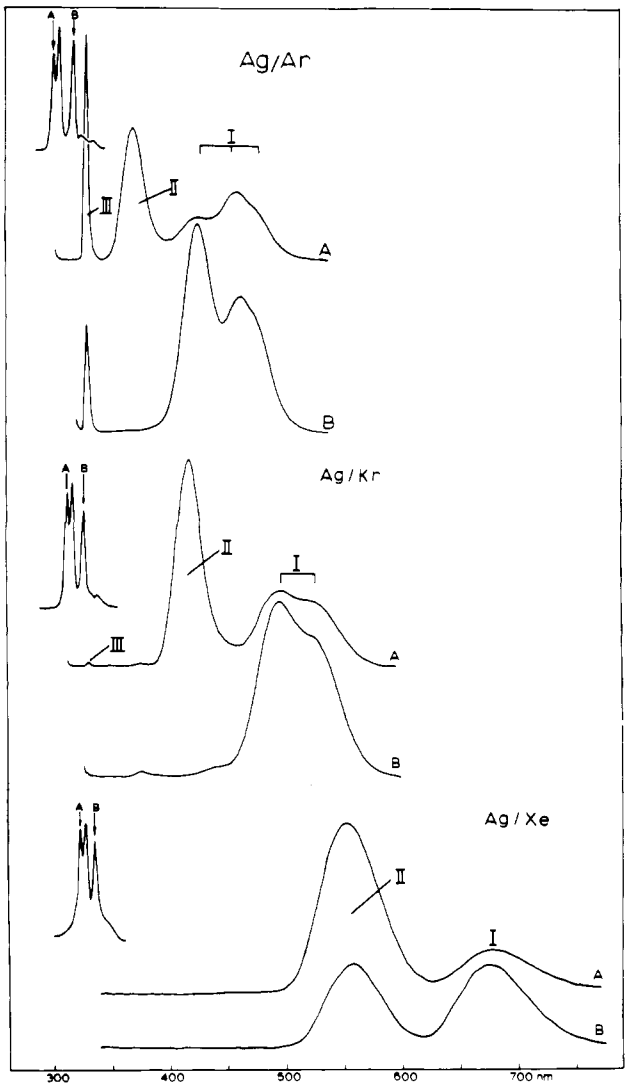

Figure 1. Comparison of the major emission bands of silver atoms isolated in Ar, Kr, and Xe matrices; the ordinate represents emission intensity in arbitrary units. The corresponding excitations are illustrated on the absorption spectra shown at left.

of the principal bands appear in Table II. In comparison to the absorption spectra, the emission bands are extremely broad, and their appearance and relative intensity depend on the excitation wavelength and the conditions of matrix preparation. Figure 1 shows two separate emission spectra for each matrix together with the corresponding absorption spectrum. The traces marked A are the spectra obtained for excitation into either component of the respective high-energy absorption doublet; identical spectra were obtained for both major high-energy excitations in all cases. The B traces are the spectra obtained for excitation into the low-energy component of the respective absorption triplet. In the cases of Ar and Kr matrices, two major emission band systems with large spectral shifts can be identified. In both cases, the long-wavelength emission bands produced by the low-energy (B) excitation constitute one system, and the second system comprises the intense emission band which appears only for the high-energy (A) excitation. Note that for Ar and Kr matrices both long-wavelength emission band systems appear together only for the A excitations, whereas for Xe matrices the two major emission bands appear for both A and B excitations. In addition to the long-wavelength bands, the Ag/Ar and Ag/Kr emission spectra show the presence of a narrow band at 326 and 328 nm, respectively. As shown in Figure 1, this band is rather strong in the case of Ar matrices, quite weak for Kr matrices, and entirely absent in the case of Xe matrices. A number of additional bands have been observed in the emission spectra. As discussed later, these bands appear to be associated with unstable silver atomic trapping sites.

(19) Kenney-Wallace, G. A.; Wilson, J. P.; Farrell, J.; Gupta, B. K. *Talanta*, in press.
(20) Hulse, J. E. Ph.D. Dissertation, University of Toronto, 1979.
(21) Forstmann, F.; Kolb, D. M.; Schulze, W. *J. Chem. Phys.* **1976**, *64*, 2552.

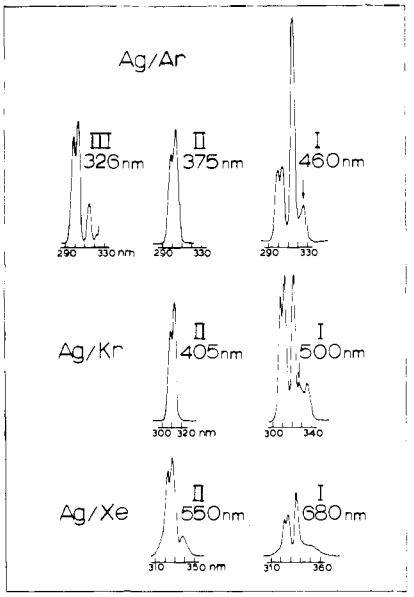

Figure 2. Fluorescence excitation spectra for the major emission bands shown in Figure 1 (see also Table III). The ordinate represents emission intensity in arbitrary units. The corresponding emission wavelengths are indicated beside each spectrum.

Table III. Fluorescence Excitation Spectra of Silver Atoms in Rare Gas Matrices[a]

matrix	excitation maxima, nm		
	326 nm (III)	375 nm (II)	460 nm (I)[b]
Ar	299, 304 315, 322	299, 304	299, 304 315, 326
		405 nm (II)	500 nm (I)[b]
Kr		309, 313	309, 313 322, 328 335
		550 nm (II)	680 nm (I)
Xe		322, 327[c] 337	322, 327[c] 335, 350

[a] The corresponding emission wavelengths are indicated with roman numerals (see Figure 1). [b] The same excitation spectrum applies for each component of the emission band system. [c] High-resolution spectra show this band to be a doublet with components at 326 and 327 nm.

Figure 2 shows fluorescence excitation spectra for the major emission bands shown in Figure 1. These spectra show explicitly the origin of the emission bands we have just described. The wavelengths of the excitation maxima are summarized in Table III. Note that in all cases the excitation spectra for the bands labeled I in Figure 1 show the presence of each major component of the respective absorption triplet (compare Tables I and III). In the cases of Ar and Kr matrices, the excitation spectra for the bands labeled II in Figure 1 show only the presence of the two high-energy components of the respective absorption triplet. These data will be important in explaining the origin of the spectral splittings later in the paper. Note that the wavelengths of the lowest energy maxima of the two Ag/Xe excitation spectra are significantly different. As shown in Table III, these excitation maxima occur at 337 and 335 nm for the II and I Ag/Xe emission bands, respectively. We note for later reference that the 335-nm maximum correlates exactly with the low-energy component of the Ag/Xe absorption spectrum (Table I). The excitation spectra for the long-wavelength Ag/Ar and Ag/Kr emission bands show the presence of maxima in addition to those corresponding to the major absorption band components. Although some of these are thermally unstable and can be almost completely eliminated by annealing, others show a thermal stability comparable to that of the principal absorption bands. An example of the former type

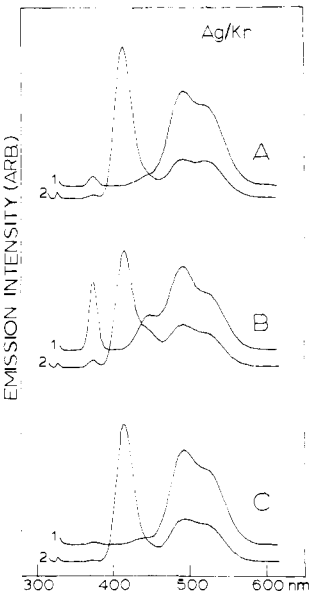

Figure 3. Emission spectra of silver atoms isolated in solid Kr at 12 K (Ag/Kr $\simeq 1/10^4$) showing the influence of UV irradiation and subsequent thermal annealing. The traces labeled 1 and 2 refer to 322 and 309 nm excitation, respectively: (A) matrix freshly deposited; (B) matrix after a 10-min irradiation at 310 nm (using the excitation system of the spectrophotometer with a 20 nm band-pass); (C) matrix after thermal annealing at 35 K subsequent to the irradiation, followed by recooling to 12 K for spectral recording.

is the 335-nm band appearing in the Ag/Kr excitation spectrum. The 337-nm Ag/Xe excitation maximum described above, and the 326-nm Ag/Ar and 328-nm Ag/Kr excitation maxima (indicated by arrows in Figure 2) are examples of the latter type. The last two examples are interesting because of the occurrence in both cases of an emission band at nearly the same wavelength, viz., 326 nm Ag/Ar and 328 nm Ag/Kr.

2. Matrix Variables. The emission spectra are in all cases very sensitive to the density of silver atoms, matrix temperature, prolonged exposure to UV radiation, and thermal annealing. The dependence of the Ag absorption spectra on the matrix conditions[13,22] is much less pronounced. The absorption spectral changes observed in the present study involved mainly variations in bandwidths and in the structure and relative intensity of the weak side bands. In no case was a significant change observed in the relative intensities of the three major absorption band components.

The emission spectra undergo pronounced changes when the matrix deposits are exposed to a significant level of UV light in the region of the silver atomic absorption bands. In the case of very low density Ag atom deposits (e.g., Ag:Kr $\sim$ 1:10[4]) in Kr or Xe, these spectral changes can be exactly reversed by thermal annealing. However, in higher silver density systems (e.g., Ag/Kr $\sim$ 1:10[3]) the UV irradiation causes an irreversible change resulting in a marked drop in the total fluorescence intensity. Concurrent changes in the absorption spectra confirm that the loss of emission intensity is due to photoinduced diffusion/aggregation processes[6,7] of the entrapped silver atoms. Figure 3 shows the effects of UV irradiation and subsequent thermal annealing for the case of low Ag density Kr matrices. Note that the UV exposure causes decay of the major emission bands but pronounced growth of the bands near 375 and 450 nm. As shown in the lower traces of Figure 3, subsequent thermal annealing restores the system to its original profile of wavelength-dependent emission intensities. In contrast, when the high density Ag/Ar system is similarly treated, the UV irradiation produces irreversible changes in the intensities of the emission peaks, as illustrated in Figure 4. The only significant effect of subsequent thermal annealing is elimination of the weak band near 360 nm. (It should be noted that this thermally unstable

(22) Schulze, W.; Kolb, D. M.; Gerischer, H. *J. Chem. Soc., Faraday Trans. 2*, **1975**, *71*, 1763.

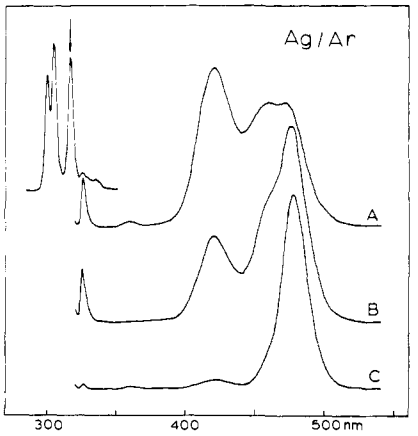

Figure 4. Emission spectra of silver atoms isolated in solid Ar at 12 K showing the influence of UV irradiation; the ordinate represents emission intensity in arbitrary units. The corresponding excitation (315 nm) is indicated on the absorption spectrum shown at upper left: (A) matrix freshly deposited (Ag/Ar $\simeq 1/10^4$); (B) matrix after a 20-min irradiation at 300 nm (using the excitation system of the spectrophotometer with a 20-nm band-pass); (C) emission spectrum obtained after prolonged 300-nm irradiation ($\simeq$1 h) in a separate experiment (Ag/Ar $\simeq 1/10^3$).

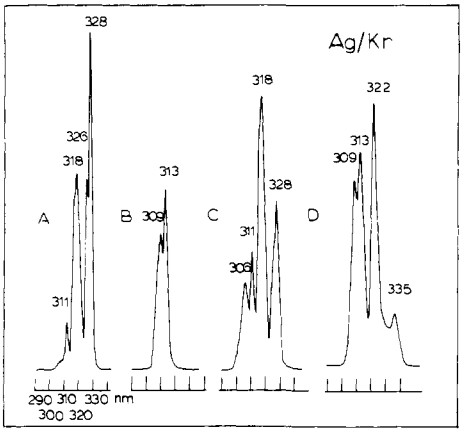

Figure 5. Fluorescence excitation spectra of silver atoms isolated in freshly deposited Kr matrices at 12 K (Ag/Kr $\simeq 1/10^4$); the ordinate represents emission intensity in arbitrary units. The wavelengths of the excitation maxima are indicated: (A) viewed at 375 nm; (B) viewed at 405 nm; (C) viewed at 450 nm; (D) viewed at 500 nm.

band is shifted slightly from the major emission band at 367 nm—see Figure 1.) The lower trace of Figure 4 shows an emission spectrum obtained after prolonged UV irradiation in a separate experiment. Note the markedly different intensity profile as compared to trace A of Figure 4. These results demonstrate that the long-wavelength emission band system of silver atoms in Ar matrices is extremely sensitive to the matrix conditions, especially as regards exposure to UV light.

Figure 5 shows fluorescence excitation spectra for the Ag/Kr emission bands illustrated in Figure 3. Note that at least nine distinct absorption (excitation) maxima can be distinguished and that traces A and C, corresponding to the thermally unstable Ag/Kr emission bands, do *not* show the presence of the primary absorption maxima at 309, 313, and 322 nm. As discussed in a later section of this paper, the ^2P excited state of the silver atoms can be split at most threefold in the absence of a magnetic field. The results shown in Figures 3 and 5 are therefore strongly suggestive of secondary silver atom trapping sites having distinct absorption and emission bands. The absence of the major absorption maxima in the excitation spectra for the 375- and 450-nm Ag/Kr emission bands indicates that these emissions originate exclusively from excitation of secondary silver atom trapping sites.

The emission spectra exhibit a reversible temperature dependence in all cases. The effects are most pronounced for Ar matrices,[2b] where there appear to be two ranges of temperature

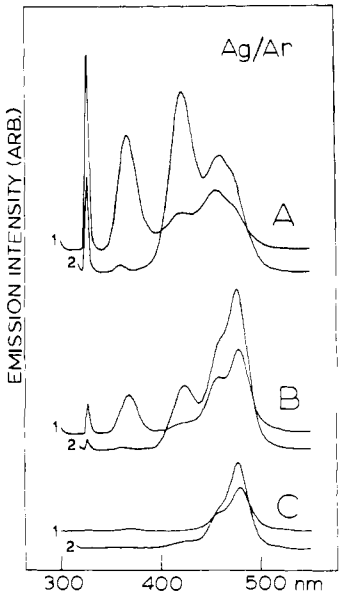

Figure 6. Emission spectra of silver atoms isolated in Ar matrices at 12 K showing the influence of the concentration conditions. The traces labeled 1 and 2 refer to 299- and 315-nm excitation, respectively. The corresponding absorption spectra (not illustrated) show that roughly equal numbers of isolated silver atoms were present in each case: (A) Ag/Ar $\simeq 1/2 \times 10^4$; (B) Ag/Ar $\simeq 1/2 \times 10^3$; (C) Ag/Ar $\simeq 1/1 \times 10^3$.

dependence. For the case of a dilute, well-annealed Ar matrix showing emission spectra similar to those illustrated in Figure 1, raising the temperature from 12 to ~20 K causes a dramatic reversal in the relative intensities of the 423- and 457-nm emission bands. A further increase in temperature to ~30 K causes a very pronounced drop in the intensity of the band near 326 nm and an increase in intensity of the long-wavelength emission bands. These temperature effects are entirely reversible. The Ag/Kr and Ag/Xe emission spectra show similar but less pronounced temperature-induced variations, including relative band intensity changes and slight broadening and energy shift effects. In all cases, the long-wavelength emission bands tend to be favored at higher matrix temperatures. No tendency for thermal quenching of the luminescence was observed for any of the rare gas matrices.

A number of concentration-dependent effects have been observed in the emission spectra, including a pronounced quenching of the luminescence at higher silver concentrations. The effect is illustrated for the case of Ar matrices in Figure 6, which shows emission spectra for three Ag/Ar deposits of differing Ag densities. The corresponding absorption spectra confirmed that roughly equal numbers of isolated silver atoms were present in each matrix. The pronounced decrease in luminescence intensity illustrated in Figure 6 shows that concentration quenching effects are important in these matrix-emission spectra. It is interesting to note that the high-energy Ag/Ar emission bands tend to disappear first as the concentration of silver increases. Similar results have been obtained for Kr and Xe matrices. In the case of Xe, a new emission band appears near 480 nm under high concentration conditions. However, all fluorescence is completely quenched at concentrations above Ag/Xe $\simeq 1/5 \times 10^2$, although atomic absorption persists.

3. Polarization and Lifetime Measurements. A study of the degree of polarization of the luminescence was carried out by use of film polarizers in the excitation and emission beams. The polarization, P, can be expressed as

$$P = (I_{\parallel} - I_{\perp})/(I_{\parallel} + I_{\perp})$$

where $I_{\parallel}$ and $I_{\perp}$ are the emission intensities measured for parallel and perpendicular orientations of the emission polarizer relative to the vertical excitation polarizer. The measured values of P, which were corrected for instrumental factors,[23] fell within limits

(23) Azumi, T.; McGlynn, S. P. *J. Chem. Phys.* **1962**, *37*, 2413.

of $P_{obsd} = 0 \pm 0.05$, and thus the emission bands were completely depolarized in all matrices.

Preliminary lifetime measurements were made in the Ag/Xe system following pulsed laser excitation at 337.1 nm. It is clearly of great importance to know the time dependence of the emissions observed following Ag atom excitation, and to determine whether or not all the emission bands are present simultaneously or grow in at different time intervals. Transient fluorescence signals were recorded for the dilute Ag/Xe system at 550 and 680 nm. All the fluorescence signals appeared within the nanosecond time resolution of the detection equipment and decayed exponentially with time. The lifetime measured for τ^* was 28 ± 3 ns at 550 nm and 56 ± 5 ns at 680 nm, respectively, in the dilute Ag/Xe matrix.

Discussion

1. ^2D–^2S Transition. The highest energy emission band of Ag atoms in Ar and Kr matrices (326 nm/Ar and 328 nm/Kr) is assigned as the $4d^95s^2\ ^2D_{5/2} \rightarrow 4d^{10}5s^1\ ^2S_{1/2}$ silver atomic transition, which is formally forbidden by the parity and J selection rules. There are two main lines of evidence which support this assignment. In the first place, the analogous transition appears weakly at 330.7 nm in the arc spectrum of silver vapor.[26] Thus even in the gas phase the forbidden transition acquires some intensity. Second, the emission spectra of Cu[27] and Au[2b] atoms isolated in Kr matrices, excited at the $^2P \leftarrow {}^2S$ resonance absorption frequencies, exhibit intense emission bands which can be unambiguously assigned as the corresponding $nd^9(n+1)s^2\ ^2D_{3/2} \rightarrow nd^{10}(n+1)s^1\ ^2S_{1/2}$ transitions. The important point is that $^2D \rightarrow {}^2S$ radiative transitions occur following optical excitation of the Cu or Au ^2P levels. A similar process might therefore be expected in the Ag system. We note here that a $^1D \rightarrow {}^1S$ transition has been observed for Ca atoms isolated in Ar matrices.[4] The energy level structures of Cu, Ag, and Au atoms differ in that only for Ag atoms does the lowest $^2D_{3/2}$ state lie higher in energy than the uppermost level of the valence ^2P manifold,[12] leaving only the $^2D_{5/2}$ component at lower energy. In Cu and Au atoms both the $^2D_{3/2}$ and $^2D_{5/2}$ states lie well below the ^2P levels. It may also be noted that in all cases there are no other levels lying intermediate between the ground ^2S and the valence ^2P states. The occurrence of a $^2D_{3/2} \rightarrow {}^2S_{1/2}$ transition in Cu and Au atoms but a $^2D_{5/2} \rightarrow {}^2S_{1/2}$ transition in Ag atoms, following $^2P \leftarrow {}^2S$ photoexcitation, can therefore be understood in terms of the accessibility of the $^2D_{3/2}$ and $^2D_{5/2}$ levels from the optically excited ^2P states.

The variation in the intensity of the $^2D_{5/2} \rightarrow {}^2S_{1/2}$ Ag atomic emission band in Ar, Kr, and Xe matrices can be interpreted in terms of a competition between the various relaxation channels available to the excited Ag atoms. The nature of the processes which compete with the $^2D \rightarrow {}^2S$ transition and which appear to be dominant in the cases of 12 K Kr and Xe matrices and 30 K Ar matrices, respectively, is considered in the following sections of the paper. In concluding the discussion of the ^2D–^2S transition we note that certain Ag/Ar and Ag/Kr excitation spectra (Figure 2) show maxima at nearly the same wavelength as the corresponding $^2D_{5/2} \rightarrow {}^2S_{1/2}$ emission band, as previously described. This coincidence of excitation and emission band maxima is either fortuitous or it means that the same electronic transitions are being observed in absorption and in emission, with essentially no Stokes shift. The occurrence of weak $^2D_{5/2} \leftarrow {}^2S_{1/2}$ absorption maxima for Ag atoms in Ar and Kr matrices would have important implications for the interpretation of the Ag/Xe absorption spectrum, which consists of four strong components. The appearance of four components for Ag/Xe instead of the three observed for Ar and Kr matrices has previously been interpreted by Brewer et al.[28] in terms of a $^2D_{3/2} \leftarrow {}^2S_{1/2}$ transition and by Forstmann et al.[21] in terms of a Ag/Xe covalent interaction.

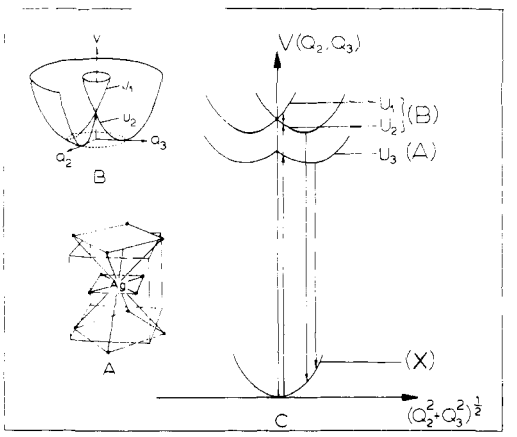

Figure 7. (A) Representation of a tetragonal distortion of a tetradecahedral complex. The extremal geometry has D_{4h} symmetry (from ref 29c). (B) Schematic potential energy surface for a doubly degenerate electronic state (in O_h symmetry) interacting with a doubly degenerate vibrational mode, neglecting anharmonic effects. V represents the nuclear potential energy and Q_2 and Q_3 represent the degenerate components of an E_g vibrational mode (from ref 29a). (C) Schematic representation of the ground- and excited-state potential energy surfaces for AgX_{12} complexes (where X is Ar, Kr, or Xe). Q_2 and Q_3 are "quasi-molecular" normal coordinates corresponding to the degenerate components of an E_g vibrational mode. The excited-state surfaces have trigonally disposed minima representing equivalent tetragonal distortions along the x, y, and z directions. The absorption and emission processes are illustrated.

2. Vibronic Coupling Model. In the following sections we interpret the observations described above in terms of a Jahn–Teller effect operative in the degenerate electronic state of the excited silver atoms, where the metal atomic centers and nearest neighbor rare gas atoms are treated as "quasi-molecular" systems (local vibrational mode approximation as described in ref 29a). As a structural model for the major trapping sites of silver atoms in Ar, Kr, and Xe solids, we assume that the matrices exhibit local order to the extent that the silver atoms occupy substitutional sites of normal fcc noble gas lattices. The metal atoms are therefore 12-coordinate and the local structure is tetradecahedral, having octahedral symmetry. Support for this structural model may be found in the results of ESR studies of Cu, Ag, and Au atoms[30] and Mn^+ and Cr^+ ions[31] isolated in rare gas matrices.

The $5p^1\ ^2P \leftarrow 5s^1\ ^2S$ electronic transition of free silver atoms is split by spin–orbit coupling into $^2P_{1/2}$ and $^2P_{3/2}$ components, with an interval of 920.7 cm^{-1}.[12] The spin–orbit levels transform as $^2E_{1/2}$ and $^2G_{3/2}$ in the octahedral symmetry of the rare gas host lattice. The $^2E_{1/2}$ state is doubly degenerate (Kramers doublet) and the $^2G_{3/2}$ state is fourfold degenerate (comprising two degenerate Kramers doublets). Now the Jahn–Teller theorum states unequivocally that a $G_{3/2}$ electronic state is unstable and that there exists a nontotally symmetric structural distortion which lifts the electronic degeneracy and results in a net stabilization of the complex. The vibrational modes that can couple in first order with a $G_{3/2u}$ state are contained in the antisymmetric square[29b] $\{G_{3/2u}{}^2\} = A_{1g} + E_g + T_{2g}$. Coupling with E_g modes stabilizes tetragonal distortions (see Figure 7A) and coupling with T_{2g} modes stabilizes trigonal distortions.

Jahn–Teller effects have previously been invoked to interpret the splittings seen for the spin-states $^2P_{1/2,3/2}$ of Na and $^3P_1$ of Hg in Ar matrices.[14c] A detailed theoretical treatment of the dynamic Jahn–Teller effect for the ground state ($^2P_{1/2}$) of Al, Ga, and In atoms in rare gas matrices[5] considered the E_g and T_{2g} vibrational modes of a tetradecahedral site (such as we propose

(24) Ozin, G. A.; Huber, H.; Mitchell, S. A. *Inorg. Chem.* **1979**, *18*, 2932.
(25) Ozin, G. A.; Huber, H.; Mitchell, S. A., manuscript in preparation.
(26) Shenstone, A. G. *Phys. Rev.* **1940**, *57*, 894.
(27) Farrell, J.; Kenney-Wallace, G. A.; Mitchell, S. A.; Ozin, G. A., unpublished results.
(28) Brewer, L.; King, B. *J. Chem. Phys.* **1970**, *53*, 3981.
(29) (a) Sturge, M. D. *Solid State Phys.* **1967**, *20*, 91. (b) Englman, R. "The Jahn–Teller Effect in Molecules and Crystals"; Wiley: New York, 1972. (c) Liehr, A. D. *J. Phys. Chem.* **1963**, *67*, 389.
(30) Kasai, P. H.; McLeod, D., Jr. *J. Chem. Phys.* **1971**, *55*, 1566.
(31) Kasai, P. H. *Phys. Rev. Lett.* **1968**, *21*, 67; *Acc. Chem. Res.* **1971**, *4*, 329.

here) and suggested that for Al, at least, the E_g modes were dominant. On the other hand, in the earliest discussion of an F-center model to explain both absorption *and* emission spectra of Li in rare gas matrices, it was concluded that although both modes were active, the T_{2g} was dominant.[14b] More recently the MCD data for Mg atoms in Ar matrices have been interpreted in a Jahn–Teller framework again emphasizing the T_{2g} mode, while the optical absorption properties of matrix-isolated Cu atoms have also been interpreted in a similar F center vein.[20]

The vibronic problem involving a $^2T_{1u}$ electronic state subject to strong spin–orbit forces has been fully discussed by Moran[32a] and by Fulton and Fitchen[32b] in connection with the optical absorption spectra of F centers in cesium halides. These papers provide a theoretical framework within which many of the optical and photolytic properties we observe for matrix-entrapped silver atoms can be understood. The usefulness of the F center model to the problem presently under consideration stems from the fact that the nearest neighbor shell has O_h symmetry both for F centers (single electrons trapped in anion vacancies of alkali halide crystals) and for silver atoms trapped in substitutional sites of fcc rare gas lattices. As described in the papers[32] cited above, the initial assumption of the model involves neglecting the interactions with T_{2g} modes and considering only a single E_g mode. A further simplification is achieved by assuming that the spin–orbit coupling is much more important than the vibronic interaction.

The potential energy surface for a doubly degenerate electronic state (in O_h symmetry) interacting with a degenerate vibrational mode, assuming harmonic potentials and considering only first-order vibronic interactions,[29] is illustrated in Figure 7B. The upper and lower branches of the potential surface, labeled U_1 and U_2, represent the two electronic states which replace the originally degenerate state. Referring specifically to the $G_{3/2}$ level of the excited silver atoms, the separation of the U_1 and U_2 branches at any point in the (Q_2, Q_3) plane represents the vibronic splitting of the $G_{3/2}$ excited state, where Q_2 and Q_3 represent the degenerate components of the local E_g vibrational mode. If anharmonic terms are included in the expansion of the nuclear potential energy, then the surface of Figure 7B loses its cylindrical character and retains only the threefold symmetry arising from the cubic symmetry of the Hamiltonian (the cubic potential is symmetrical in the x, y, and z directions). In this case the potential surface has three equivalent trigonally disposed minima, separated by saddle points.[29] These minima correspond to equivalent tetragonal distortions along the x, y, and z directions.

The analysis described thus far has been confined to vibronic coupling effects associated with the $^2P_{3/2}$ spin–orbit component. The implicit assumption is that the spin–orbit splitting is very large relative to the vibronic interactions. If the vibronic and spin–orbit effects are comparable, then it is no longer justifiable to consider only the $^2P_{3/2}$ state since the noncubic potentials introduced by the E_g vibrations tend to mix the two spin–orbit components. Moran[32a] takes account of the effects of $^2P_{3/2}$–$^2P_{1/2}$ mixing by means of a second-order perturbation calculation. Qualitatively, the interaction has the effect of increasing the separation between the $E_{1/2}(^2P_{1/2})$ state and the centroid of the split $G_{3/2}(^2P_{3/2})$ state. The corresponding potential energy surfaces undergo a mutual repulsion which tends to increase with increasing values of Q_2 and Q_3. At the origin of the (Q_2, Q_3) plane the electrostatic potential has cubic symmetry so that no $^2P_{3/2}$–$^2P_{1/2}$ mixing occurs. A highly schematic representation of the ground- and excited-state potential energy surfaces is shown in Figure 7C.

As the schematic configuration coordinate diagram of Figure 7C will be used in subsequent discussions, it is important to establish the extent to which the qualitative features of the diagram are dependent upon the assumptions and approximations of the model.

It was assumed at the outset that the dominant vibronic coupling involves E_g rather than T_{2g} vibrational modes. Accordingly, the potential energy surfaces are drawn in the space of the Q_2 and Q_3 components of an E_g vibrational mode. We shall not consider the case of dominant T_{2g} mode coupling. As described above, the model is based on a strong spin–orbit coupling limit, with second-order corrections arising from the interaction between the spin–orbit components. The opposite limit where vibronic coupling is much more important than the spin–orbit interaction would predict a single Gaussian absorption band[32b] and is therefore inappropriate to the present problem. It is probable that an intermediate situation would best describe the case of matrix-isolated silver atoms. Figure 7C should provide an adequate representation of the potential energy surfaces for this case. Finally, we note that since all of the (non-Kramers) degeneracies have been removed in the present approximation, the inclusion of, for example, weak coupling with T_{2g}, A_{1g}, or other E_g modes should not affect Figure 7C in any important qualitative way.[32]

3. Optical and Photolytic Properties. The manner in which the threefold splitting of the absorption band arises, according to the vibronic coupling model, is illustrated in Figure 7C. The vertical line representing the Franck–Condon absorption process is displaced from the origin of the (Q_2, Q_3) plane because the maximum in the probability distribution of the ground-state vibrational wave function occurs not at the origin but at $(Q_2^2 + Q_3^2)^{1/2} = 2^{-1/2}\alpha^{-1}$.[33] Hence, vertical transitions from the ground state cross three excited-state potential energy surfaces, resulting in a threefold splitting of the optical absorption band.

Forstmann et al.[13] have described the temperature dependence of the absorption spectra of silver atoms isolated in rare gas matrices. The observed splittings generally increase and the bands broaden as the temperature of the matrix is raised. Both of these effects are readily understood within the framework of the vibronic coupling model. As the temperature is raised, the root mean square tetragonal distortion of the ground-state complex tends to increase because of the increased amplitude of the E_g vibrations at higher temperatures. Thus, the maximum in the probability distribution of the vibrational wave function is effectively moved to larger displacements from the origin of the (Q_2, Q_3) plane. As can be seen in Figure 7C, this has the effect of increasing the effective separation between the U_1 and U_2 excited-state potential energy surfaces, resulting in an increased splitting between the corresponding components of the absorption spectrum. The results of Forstmann et al.[13] are in accord with the expectation based on Figure 7C in that the increased splitting is most pronounced for the high-energy absorption doublet. The broadening of the absorption bands at higher temperatures can be understood in a standard way in terms of the vibrational levels of the ground-state complex.

It was argued in the previous section that the excited-state complex should be unstable in the symmetrical configuration and that a tetragonal distortion would stabilize the complex by relieving the degeneracy of the $^2P_{3/2}$ state. These considerations lead to the following expectation concerning the relaxation behavior of the excited states. Optical excitation to the U_1, U_2, or U_3 levels should be followed by vibrational relaxation to the minimum point of the respective potential energy surface and subsequent radiative decay to the ground state surface. These processes are illustrated in Figure 7C. The large spectral shifts of the emission bands, representing profiles of the Franck–Condon factors between the initial and final states, are seen to be a consequence of the tendency for distortion of the excited-state complex. As shown in Figure 7C, the shifts arise both from the stabilization of the excited state and the accompanying destabilization of the ground state.

The destabilization caused by producing ground-state complexes in the relaxed excited-state configuration is the probable driving force for photoinduced diffusion of the silver atoms. The repulsive forces generated at the photolytic centers can apparently cause the entrapped silver atoms to undergo "jumps" to adjacent lattice sites. The diffusion process can also be thought of as the result

(32) (a) Moran, P. R. *Phys. Rev.* **1965**, *137*, A1016. (b) Fulton, T. A.; Fitchen, D. B. *Ibid.* **1969**, *179*, 846.

(33) Although the probability *density* is maximum at the origin, the element of area in the (Q_2, Q_3) plane shrinks to zero there, and hence the maximum in the probability *distribution* over the (Q_2, Q_3) plane is displaced from the origin (see ref 29a, p 188).

of a local heating effect caused by dissipation of the ground-state destabilization energy in the form of localized lattice vibrations. In this connection, it is interesting to note that the results of mixed-metal matrix photoaggregation experiments[9b] suggest that matrix heating effects are localized near the photolytic sites. It is clear that much remains to be learned of the detailed mechanism of photoinduced diffusion of matrix-entrapped metal atoms. Further studies involving spectroscopic and photoaggregation kinetic experiments are planned for the future.

A striking feature of the emission spectra of silver atoms isolated in Ar, Kr, and Xe matrices is the systematic trend toward larger spectral shifts for the heavier and more polarizable rare gas atoms (see Figure 1). This trend is indicative of an increasing stability of the excited-state complexes along the series from Ar to Xe, arising from stronger van der Waals type binding forces for the more polarizable rare gases. A larger binding energy will of course be reflected in a deeper potential energy well and, accordingly, a larger contribution to the spectral shift from the stabilization of the excited state. It can be seen in this way that the observed trend in the spectral shifts provides a strong indication that van der Waals type complexes are formed between the optically excited silver atoms and the neighboring rare gas atoms. Thus, the existence of a stabilization energy associated with a static Jahn–Teller distortion of the excited-state complexes can be understood in these terms.

Although some remarkable differences have been noted among the spectra obtained for the three rare gas matrices, there are also a number of important common features: (1) the occurrence in all cases of two major emission band systems exhibiting large spectral shifts (the longer wavelength system showing structure in the cases of Ar and Kr matrices); (2) the appearance in all cases of virtually identical emission spectra for the two high-energy excitations (U_1 and U_2), yet different spectra for the low-energy excitation (U_3); (3) the complete depolarization of the luminescence in all cases. In the following paragraphs we show how these three common features can be understood within the framework of the vibronic coupling model.

According to the arguments of the previous section, both the upper and lower excited-state potential energy surfaces (labeled B and A in Figure 7C) should have trigonally disposed minima representing equivalent tetragonal distortions along the x, y, and z directions. Another important topographical feature of the upper potential energy surface (labeled B) is the continuity between the U_1 and U_2 branches. It is apparent from these considerations that the vibrational relaxation processes following excitation to the U_1 and U_2 branches must lead to fully equivalent structural configurations of the relaxed excited state, since both branches of the potential energy surface have common minimum points. Therefore, the same emission spectrum should be produced for both U_1 and U_2 excitations. Moreover, it is clear that a different spectrum should in general be expected for the U_3 excitation. In the absence of nonradiative transitions between the excited-state surfaces, single emission bands would be expected for both the U_1 and U_2 excitations and the U_3 excitation. This is the proposed origin of the two major emission band systems.

It can now be seen that the appearance of both major emission band systems for the high-energy (U_1 and U_2) excitations in Ar, Kr, and Xe matrices, as previously described, implies that nonradiative transitions can occur between the upper (B) and the lower (A) potential energy surfaces. The occurrence of temperature-dependent nonradiative transitions could account for some of the temperature effects described earlier. The broadly structured appearance of the long-wavelength Ag/Ar (423, 457, 478 nm) and Ag/Kr (495, 525 nm) emission bands (see Figure 1) is more difficult to explain, although the sensitivity of the structure to the matrix conditions suggests that multiple trapping site effects are involved. It is possible, for example, that lattice inhomogeneities render the three possible tetragonal distortions of the trapping site inequivalent and thereby cause a splitting of the emission bands. An alternative possibility is that trigonal distortions may in favorable cases occur through strong coupling with T_{2g} vibrational modes. Although it is possible that this could account for some of the observed splittings, it is not clear exactly how the emission spectra would be affected.

The emission spectra of Ag atoms in Xe matrices appear to be anomalous in that both major emission bands appear for the lowest energy (U_3) excitation, while only the longest wavelength system appears for the analogous Ar or Kr excitation (Figure 1). However, as previously mentioned, the excitation spectra shown in Figure 2 indicate that the higher energy Ag/Xe emission band originates not with the major U_3 excitation at 335 nm but with a neighboring absorption band at 337 nm, which presumably arises from secondary trapping site effects. It can therefore be seen that the trend in the excitation dependence of the Ag/Ar and Ag/Kr emission spectra holds also for Xe matrices, since the only primary site excitations which produce the higher energy Ag/Xe emission band are those corresponding to the high-energy absorption doublet.

The potential for three equivalent tetragonal distortions of the excited-state complex along the x, y, and z directions suggests an explanation for the observed fluorescence depolarization. Since the states produced by optical excitation are highly vibrationally excited levels of a distorted configuration, there exists the possibility of fluxionality in the excited state. Thus, as long as the system has sufficient vibrational excitation to surmount the energy barriers, interconversions between differently oriented configurations can occur (dynamic Jahn–Teller effect). In this way, all memory of the polarization of the incident photons is lost, and the fluorescence is completely depolarized. We note that other mechanisms, for example, energy transfer, could account for the fluorescence depolarization. Although photoselection theory[34] predicts depolarized emission from randomly oriented octahedral molecules, the applicability of the theory is uncertain in the case of matrix-isolated Ag atoms. We shall defer these problems for future study and note simply that the form of the potential energy surfaces illustrated in Figure 7B,C provides a possible explanation for the observed fluorescence depolarization.

The results of the time-resolved study of the Ag/Xe emission bands provide valuable information on the dynamical behavior of the excited states. When the characteristic decay times (28 ± 3 ns at 550 nm and 56 ± 5 ns at 680 nm) are corrected for emission frequency and refractive index effects, they agree to within a factor of 2 with the mean radiative lifetime of the $^2P_{3/2}$ level of free silver atoms (6.5 ± 0.6 ns).[35] This result suggests that the fluorescent states decay exclusively by the observed radiative pathways, since lifetimes significantly shorter than the free atom value would be expected if concurrent nonradiative decay processes were important. Of course, nonradiative processes other than those leading to the fluorescent states could occur in the states populated directly by light absorption. In this connection, the time-resolved measurements reveal only that both fluorescent states are formed well within nanoseconds following excitation of the silver atoms. This result is consistent with the expectation on the basis of the vibronic coupling model for the relaxation of the excited states.

Summary

We have shown that a model involving vibronic coupling between the $^2P_{1/2,3/2}$ spin–orbit components of atomic silver and the allowed distortion modes of the rare gas atoms comprising the tetradecahedral (major) trapping site leads to a unified description of the absorption and emission and diffusion/aggregation properties of silver atoms isolated in rare gas matrices. For the case of strong spin–orbit interaction and relatively weak vibronic coupling involving a single E_g cage vibrational mode, a configurational coordinate ground- and excited-state potential energy diagram can be constructed, which permits a fairly comprehensive interpretation of the major findings for atomic silver guests in rare gas solid hosts. The threefold splitting and temperature dependence of the absorption spectra, the overall structure and excitation dependence of the emission spectra, and the occurrence of pho-

(34) Albrecht, A. C. *J. Mol. Spectrosc.* **1961**, *6*, 84.
(35) Klose, J. Z. *Astrophys. J.* **1975**, *198*, 229.

toinduced diffusion and clustering of the silver atoms can all be qualitatively understood. Although the successful interpretation of the absorption and emission spectra suggests that the main features of the potential energy surfaces are adequately described, the data do not permit a conclusive demonstration of the importance of the Jahn–Teller effect. The vibronic model is attractive, however, because unlike the crystal field model,[13] it does not require the assumption of lower than octahedral symmetry for the ground-state silver atom trapping site. This is an inherent difficulty of the crystal field approach, because it is not readily apparent why substitutionally incorporated ^2S Ag atoms should occupy axially distorted tetradecahedral trapping sites.

It is clear that many problems remain for future research in this area. In particular, the temperature and concentration dependence of the emission spectra, the polarization properties, and the competition between $^2D \rightarrow {}^2S$ and "relaxed" $^2P \rightarrow {}^2S$ emission require further study. It is hoped that continuing research will further elucidate the photoprocesses of matrix-isolated silver atoms. An extension to silver cluster species and to other metal and matrix systems is planned for the future.

Acknowledgment. S.M. and G.A.O. acknowledge the NSERC Canada Strategic Energy, New Ideas and Operating Grants Programmes for financial support of this research. G.A.K.-W. and J.F. acknowledge the NSERC and the donors of the Petroleum Research Fund, administered by the American Chemical Society, for partial support of this project. S.M. also recognizes the NSERC for a scholarship throughout his graduate research.

Solid-State Resolution of Binaphthyl: Crystal and Molecular Structures of the Chiral (A)[1] Form and Racemic (B)[1] Form and the Study of the Rearrangement of Single Crystals. Requirements for Development of Hemihedral Faces for Enantiomer Identification

Ruth B. Kress,[2a] Eileen N. Duesler,[2a] Margaret C. Etter,*[2b] Iain C. Paul,*[2a] and David Y. Curtin*[2a]

Contribution from the Department of Chemistry, School of Chemical Sciences, University of Illinois, Urbana, Illinois 61801, and Central Research Laboratories, 3M Company, St. Paul, Minnesota 55133. *Received April 1, 1980*

Abstract: The conversion in the solid state of single crystals of the racemic (low-temperature) form of 1,1′-binaphthyl to the chiral (high-temperature) form, shown previously by Pincock and Wilson to occur in bulk samples with formation of a great predominance of one enantiomer, has been studied. When a large single crystal is subjected to temperatures and times which have been shown to cause rearrangement of crystalline racemic binaphthyl to the chiral form, crystals of the chiral form can be seen growing in the vicinity of the parent crystal but Weissenberg photographs of the parent still show the undistorted reflections of the low-temperature racemic starting material. A reaction front leading to the production of an opaque product is observed under the appropriate conditions. Infrared and X-ray powder analyses of the product show evidence of only a few percent of the chiral product. We conclude that, at least under our reaction conditions, the major reaction pathway is not a solid–solid transformation but a solid–vapor–solid process. The crystal structure of chiral 1,1′-binaphthyl has been determined by X-ray methods. Colorless tetragonal bipyramids have $a = 7.181$ (2) Å and $c = 27.681$ (10) Å, and the structure was refined to an R factor of 0.043 on the basis of 978 nonzero reflections. A new set of data for the racemic (B) form which has been determined previously was collected, and a refinement of the structure has been carried out. The conditions for the occurrence and recognition of hemihedral faces in common chiral space groups for organic compounds are discussed.

Introduction

By virtue of restricted rotation about the bond joining the aromatic ring systems, 1,1′-binaphthyl (I) exists in its stable

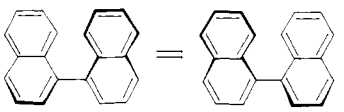

conformation as a chiral molecule. In the crystalline state it exists in two forms: the A or higher melting (159 °C) and the B or lower melting (145 °C). The B form, whose structure was determined by Kerr and Robertson,[3a] following earlier work by Brown, Trotter, and Robertson,[3b] consists of racemic crystals (space group $C2/c$) whereas the A form, whose structure has not previously been reported, was known to crystallize as a conglomerate of chiral crystals. The racemic B form is transformed on heating in the solid state to the chiral A form. An elegant and detailed study by Pincock and collaborators[4] has elucidated many features of this conversion. It is of particular interest that with ingeneously devised experimental conditions, Pincock and Wilson[4a] were able to direct the reaction to produce from essentially racemic B form the chiral A form with a high predominance of one of the two enantiomers.

(1) The racemic, low temperature form of 1,1′-binaphthyl has been called the "B" form by previous workers.[3]

(2) (a) University of Illinois. (b) 3M Company.

(3) (a) K. A. Kerr and J. M. Robertson, *J. Chem. Soc. B*, 1146 (1969); (b) W. A. C. Brown, J. Trotter, and J. M. Robertson, *Proc. Chem. Soc., London*, 115 (1961).

(4) (a) K. R. Wilson and R. E. Pincock, *J. Am. Chem. Soc.*, **97**, 1474 (1975); (b) K. R. Wilson and R. E. Pincock, *Can. J. Chem.*, **55**, 889 (1977); (c) R. E. Pincock, R. P. Bradshaw, and R. R. Perkins, *J. Mol. Evol.*, **4**, 67 (1974); (d) R. E. Pincock, R. R. Perkins, A. S. Ma, and K. R. Wilson, *Science*, **174**, 1018 (1971).

0002-7863/80/1502-7709$01.00/0